Spatial Control of Neuronal Adhesion on Diamond-Like Carbon

James M Dugan[1], Carles Colominas[2], Andrés-Amador Garcia-Granada[3] and Frederik Claeyssens[1]*

[1]Department of Materials Science and Engineering, Kroto Research Institute, The University of Sheffield, Sheffield, United Kingdom, [2]Flubetech S.L., Barcelona, Spain, [3]Grup d'Enginyeria de Productes Industrials, IQS, Universitat Ramon Llull, Barcelona, Spain

This study reports a route to spatial control of neuronal adhesion onto Diamond-Like Carbon (DLC) by surface functionalisation by poly (oligo-ethyleneglycol methacrylate) (pOEGMA) and consequent laser ablation to produce cell adhesive tracks. DLC can be deposited as a tough and low friction coating on implantable devices and surgical instruments and has favourable properties for use as a biomaterial. The pOEGMA surface coating renders the DLC surface antifouling and the laser ablation creates graphitised tracks on the surface. The surfaces were coated with laminin, which adhered preferentially to the ablation tracks. The patterned surfaces were investigated for neuronal cell growth with NG108-15 cells for short term culture and rat neural stem cells for longer term culture. The cells initially adhered highly selectively to the ablation tracks while longer term cell culture revealed a more uniform cell coverage of the surface.

Keywords: laser ablation, diamond-like carbon, poly(oligo (ethylene glycol) methacrylate), atom transfer radical polymerization, neuronal cell culture

INTRODUCTION

Brain-computer interfaces promise to revolutionise prostheses for patients suffering paralysis due to damage to the central nervous system. In human trials, ensemble recordings of neuronal activity in the primary motor cortex have been detected using microelectrode arrays (Hochberg et al., 2006). The measured signals were then digitally processed and interpreted as control signals for actuation of prosthetic devices such as robotic arms or control of a simple computer cursor. Although success has been demonstrated clinically, long term implantation of electrodes into the brain is known to cause several problems, in particular the formation of a glial scar which encapsulates the electrode and effectively acts to insulate the electrode from the target neurons, reducing the function of the electrode (Polikov et al., 2005).

Several methods have been suggested for overcoming the encapsulation of electrodes through glial scarring, including coating of the electrodes with other materials. One such material that has been proposed is Diamond-Like Carbon (DLC) (Singh et al., 2003). DLC is a form of synthetic amorphous carbon with a variable proportion of sp^3 and sp^2 bonding which can be prepared by a number of different methods including pulsed laser deposition, plasma-enhanced chemical vapour deposition and physical vapour deposition (Ohtake et al., 2021). Although DLC is an amorphous material, many of its properties resemble diamond, at least to some degree. Many of these properties make DLC highly suitable for use as a biomaterial. It exhibits a high degree of mechanical hardness, relatively low chemical reactivity, low coefficient of friction and a high degree of biocompatibility. Indeed DLC has been demonstrated as a coating for ureteral stents to prevent biofilm formation (Laube et al., 2007) and arterial stents to prevent neointimal hyperplasia and restenosis (Kim et al., 2011). One
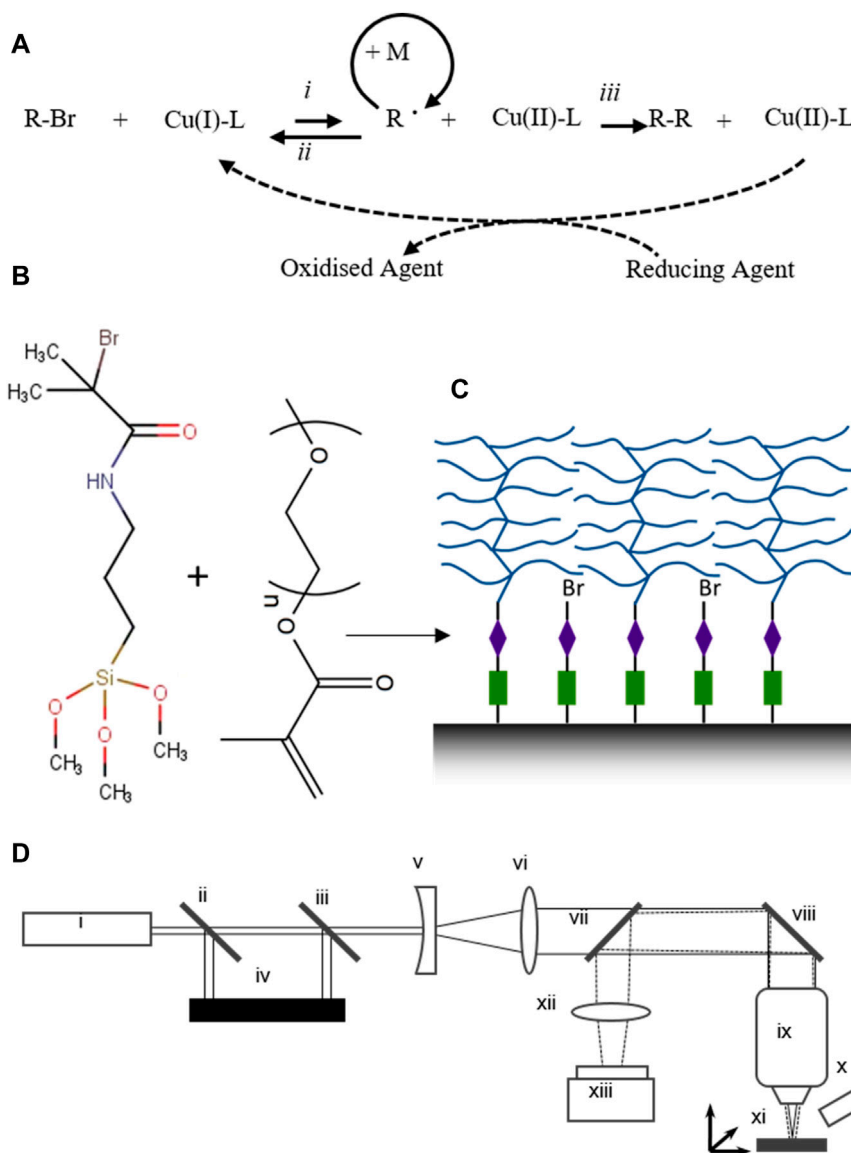
FIGURE 1 | Schematics of the various steps of the experimental procedure **(A)** the reaction scheme of ARGET ATRP used in this study (schematic adapted from (Jakubowski and Matyjaszewski, 2006)) where: (i) = activation, (ii) = deactivation and (iii) = termination. **(B)** chemical structure of the reagents used to functionalise the DLC surface and to produce the "bottle brush"-style surface pOEGMA coatings. (**(D)** Schematic of the laser ablation set-up, where, i = Nd YAG 800 ps laser (532 nm 2nd harmonic), ii = Hot mirror, iii = Variable neutral density filter, iv = Beam dump, v = plano-concave mirror, vi = convex mirror, vii = Beam sampler, viii = Silver mirror, ix = Objective lens, x = Fibre-optic xenon lamp, xi = XYZ stage, xii = Tube lens and xiii = CMOS camera.

feature of DLC which is particularly promising in this field, is the extent to which several of its properties may be modulated through doping with small quantities of additional elements introduced during the deposition process. Such an approach has been used to alter its biocompatibility in order to promote the adhesion of neurons on DLC through doping with phosphorous (Kelly et al., 2008; Regan et al., 2010). Its electrical properties may also be altered by doping with boron, indeed Pu et al. reported the transition from n-to p-type semiconductor behaviour upon increasing B-doping (Pu et al., 2010). Nitrogen doping of DLC has been reported to both

increase the adhesion of the DLC film to silicon substrates (Bootkul et al., 2014) and improve the haemocompatibility of PTFE-based implants (Srinivasan et al., 2012). Additionally, nitrogen-doped DLC films have been used for producing optical transparent electrodes (Menegazzo et al., 2011). To improve the properties of DLC as an implant material doping with F, N, Si and metals has been suggested (as summarised in Ref (Grill, 2003)).

In this study we focussed on tuning cell adhesion to DLC *via* coating the material with an antifouling layer and spatially selectively removing this layer *via* laser ablation to achieve

patterned neuronal cell adhesion (the experimental procedure is highlighted schematically in **Figure 1**). The non-fouling coating was obtained through surface initiated polymerization of brush-like coatings of polyethylene glycol by a variation of atom transfer radical polymerization (ATRP). In ATRP, a type of "living" polymerization, the vast majority of polymer chains are maintained in an inactive (or non-growing) state through use of a Copper-based catalytic system in which chain growth is catalysed by a Cu(I) species (the activating species) which is in equilibrium with a much more abundant Cu(II) species (the inactivating species) (Wang and Matyjaszewski, 1995). In the standard variation of ATRP, generation of a very low concentration of the Cu(I) catalyst occurs spontaneously *in situ*. The catalytic system is therefore very sensitive to atmospheric and dissolved oxygen. A variant of ATRP in which a reducing agent is used to generate the active Cu(I) catalyst species was developed some time later and was used in this study (Jakubowski and Matyjaszewski, 2006). The benefit is that the polymerization is much less prone to termination by oxygen and so the procedure may be carried out without the use of specialist equipment and inert gases. ATRP can be used to render surfaces non-fouling using a variety of monomers by initiating the reaction *via* a functional group that is bound to the surface (surface initiated-ATRP or SI-ATRP) (Rodriguez-Emmenegger et al., 2012; Surman et al., 2015). Polymer brushes are thought to produce non-fouling surfaces when they are well hydrated and composed of highly flexible chains (Chen et al., 2010). Here we have used monomethyl oligo-ethylene glycol methacrylate (OEGMA) in order to prepare highly non-fouling polymer brush coatings on DLC substrates.

Laser ablation was a popular route to produce novel thin films in the early 2000s (Ashfold et al., 2004) but has also has been used for applications as diverse as the fabrication of wearable microelectronic devices (Green Marques et al., 2019) and the removal of living tissue in various surgical procedures (Beck et al., 2020). Pulsed laser ablation using femtosecond pulsed Ti-Sapphire lasers has also been demonstrated as a method for fabrication of structured thin polymer films supported on substrate materials (Ibrahim et al., 2007; Doyle et al., 2009; Jeon et al., 2011). Given the high potential peak powers of such lasers and the resulting high fluences achievable with high numerical aperture optics, the mode of energy absorption in the ablation process may involve non-linear optical phenomena such as two photon absorption or higher order absorption of three or more photons simultaneously (Ibrahim et al., 2007). As the likelihood of a multi-photon absorption event scales non-linearly with light intensity, ablation of material by multi-photon absorption may allow machining resolution way below the diffraction limit. Indeed, using a 400 nm frequency doubled Ti:Sapphire laser, features as small as 80 nm in diameter have been achieved (Jeon et al., 2011).

Here we present an alternative method of pulsed laser ablation for fabrication of two-dimensional patterns within a thin polymer film supported on a surface coated with DLC. The second harmonic (532 nm, 0.45 ns pulse length) from a compact and relatively low-cost passively Q-switched Nd YAG DPSS sub-nanosecond pulsed laser (AlphaLAS) was employed to ablate

DLC. As DLC is opaque to visible light, the surface layer of the DLC was removed along with the surface coating of non-fouling pOEGMA brushes, revealing regions of material that could support extracellular matrix protein adsorption and therefore cell adhesion.

EXPERIMENTAL METHODS

Materials and Reagents
All chemicals, reagents and bioreagents were obtained from Sigma Aldrich (Dorset, UK) and were used as received unless otherwise stated. HPLC grade solvents were used for sample preparation. Silicon wafers (undoped (100) 0.9–1.5 MΩ cm 500 μm thickness single side polished) were obtained from universitywafers.com. Decon 90 was obtained from Fisher Scientific (Loughborough, UK). Phosphate buffered saline (PBS), Dulbecco's modified Eagle's medium (DMEM), fetal bovine serum (FBS) and L-glutamine were obtained from Thermo Fisher Scientific. Neurobasal medium, B27 supplement, GlutaMax supplement, penicillin/streptomycin (5,000 units and 5 mg per ml, respectively) recombinant human basic fibroblast growth factor (bFGF), Accutase, AlexFluor 488 conjugated goat-anti-mouse IgG secondary antibody, AlexaFluor 543 conjugated goat-anti-rabbit IgG secondary antibody and ProLong Gold antifade reagent were obtained from Life Technologies (Paisley, UK). Papain, hibernate E-Ca medium, premixed hibernate E/B27 medium and fresh rat embryo brain tissue were obtained from Brain Bits Ltd. (UK). The NG108-15 cell line was obtained from the American Type Culture Collection (ATCC).

Deposition of Diamond-Like Carbon
Silicon wafers were coated at Flubetech with a Diamond-Like Carbon (DLC) layer at 170°C using a CemeCon CC800/9 magnetron sputtering Physical Vapour Deposition (PVD) unit from Cr and graphite targets and acetylene gas was introduced for the top pristine DLC layer. The overall coating thickness is 4.75 μm consisting of a gradient adhesion multilayer (Cr + CrN + CrCN + CrC) plus a final amorphous carbon (a-C) layer of 1.8 μm, which exhibits a hydrogen content of approx. 18%.

Functionalisation of DLC by Surface Initiated Atom Transfer Radical Polymerization
A variation of ATRP, in which the active (Cu(I)) form of the catalyst is regenerated after termination by the action of a reducing agent, was used to functionalise DLC with pOEGMA brushes. This variation, known as activators regenerated by electron transfer ATRP (ARGET ATRP), is discussed in detail elsewhere (Matyjaszewski et al., 2006; Matyjaszewski et al., 2007). and is highlighted schematically in **Figure 1A**. The DLC was first functionalised with an alkyl bromide ATRP initiator. Silicon wafers coated with DLC were cut into 6 mm square samples and washed briefly in an ultrasonic bath containing a dilute

solution of Decon 90 (2% v/v). The samples were then rinsed five times in deionised (DI) water before being submerged in freshly prepared piranha solution (3:1 mixture by volume of concentrated H_2SO_4 and H_2O_2 (30% aq)) for 15 min. The samples were then rinsed 5 times with DI water and finally with 20 MΩ ultrapure DI water before being allowed to dry in air. The dry samples were then placed in a vacuum chamber along with an open vial containing a few drops of (3-aminopropyl) triethoxysilane (APTES). The chamber was then evacuated to approximately 5 min and then isolated for 30 min to allow adsorption of APTES vapour onto the DLC samples. The samples were then removed and placed in an oven at 110°C for 30 min. The silanised samples were then placed into individual test tubes which were sealed with rubber septa. A sufficient quantity of a mixture of α-bromoisobutyryl bromide (BIBB) (2.6% v/v) and anhydrous triethylamine (3% v/v) in anhydrous tetrahydrofuran (THF) was syringed into the tubes to completely cover the samples (~1 ml per tube). After 1 h the reaction mixture was removed and the samples were washed once in THF, three times in methanol and finally once in 20 MΩ DI water.

ARGET ATRP was carried out using the alkyl bromide functionalised DLC as the initiator (the reaction is schematically depicted in **Figures 1B,C**). Firstly, methanol (16 ml), DI water (4 ml) and polyethylene glycol methacrylate monomethyl ether (300 g/mol) (20 ml) were placed in a round bottom flask sealed with a rubber septum and degassed by sparging with nitrogen for at least 15 min. Copper (II) bromide (7.4 mg), 2,2′-dipyridyl (51.5 mg) and sodium ascorbate (65.3 mg) were then added sequentially to the flask. The mixture was stirred, with continued nitrogen sparging, until all solids were dissolved. The functionalised DLC samples were placed into test tubes sealed with rubber septa. The tubes were purged with nitrogen before enough reaction mixture was syringed over the samples to fully cover them (~1 ml per tube). The headspace was once again purged with nitrogen and the reaction was allowed to proceed for 18 h. The reaction mixture was then removed and the samples were washed three times with methanol before drying in air. The dry samples were stored in a desiccator under vacuum until required. DLC functionalised with pOEGMA brushes are labelled as "DLC-pOEGMA" in the remainder of this study.

Laser Ablation

The light source used for LA was the second harmonic (532 nm) from a subnanosecond pulsed Nd-YAG DPSS laser equipped with second harmonic generator (Alphalas, Germany) with a pulse length of 450 ps and repetition rate of 45 kHz (a schematic of the set-up is highlighted in **Figure 1D**). The beam was firstly expanded before being attenuated using an adjustable reflective neutral density filter. The beam was then passed to an objective lens (Nikon CFI Super Fluor ×20, NA 0.75) which was used to focus the beam onto the sample surface. The sample was translated in the focal plane using a programmable XYZ-stage (Aerotech, Tadley, UK). In a typical experiment, the beam was attenuated to between 1 and 10 mW average power
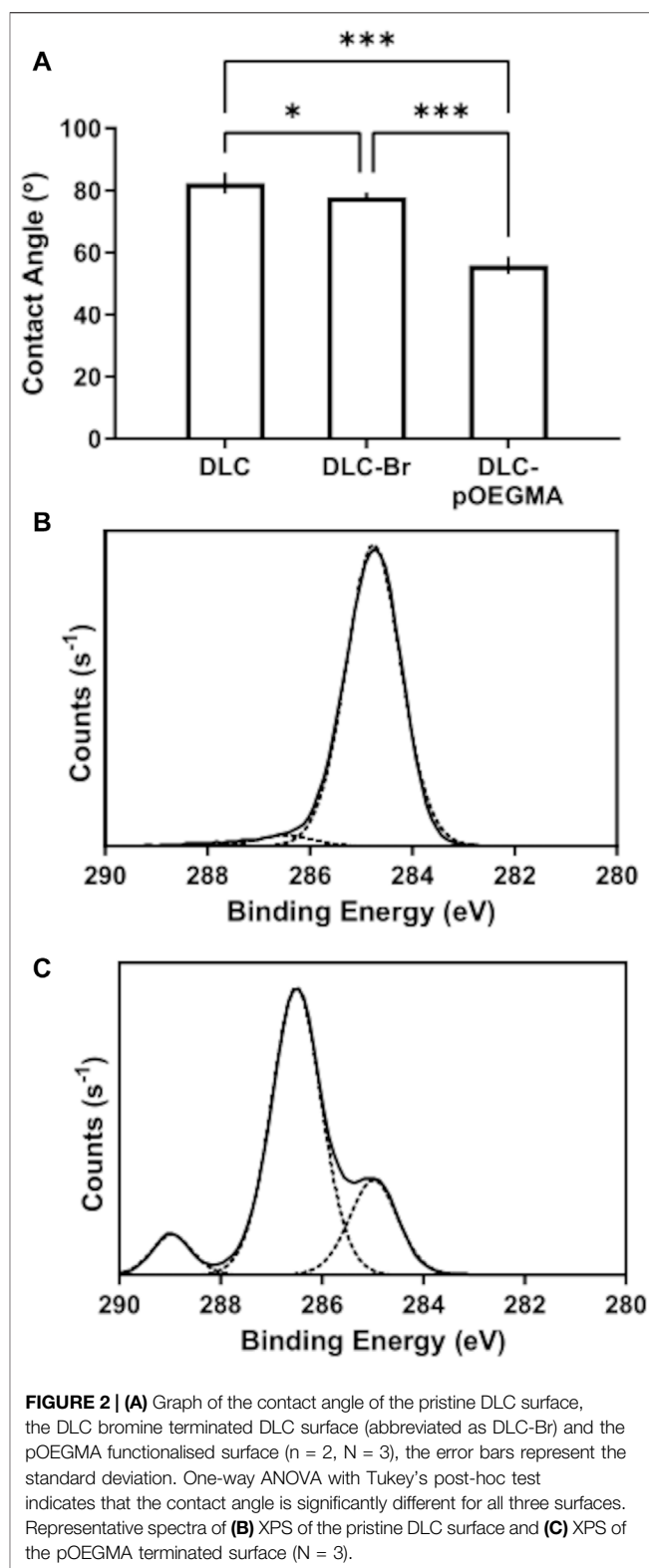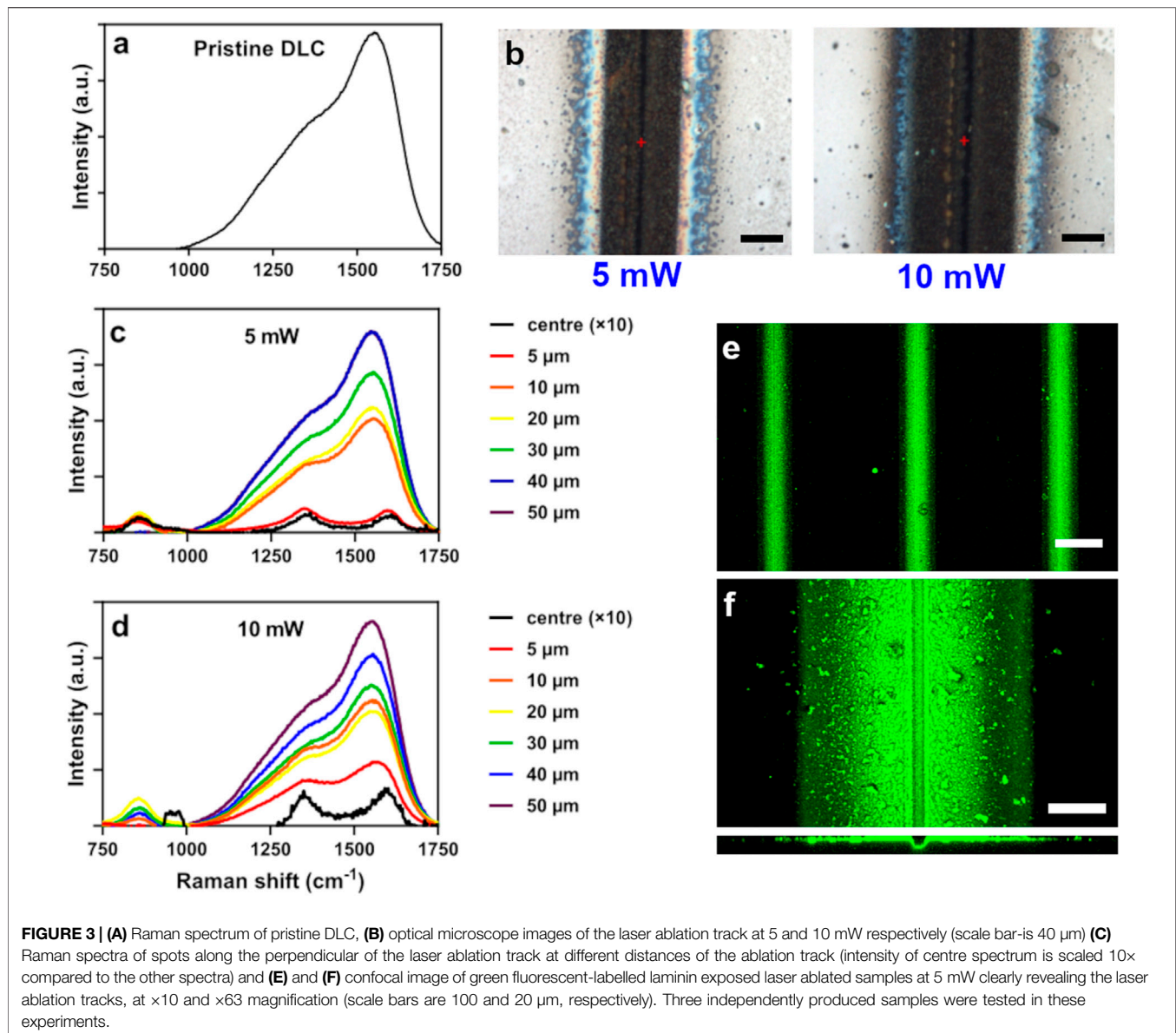

FIGURE 2 | (A) Graph of the contact angle of the pristine DLC surface, the DLC bromine terminated DLC surface (abbreviated as DLC-Br) and the pOEGMA functionalised surface (n = 2, N = 3), the error bars represent the standard deviation. One-way ANOVA with Tukey's post-hoc test indicates that the contact angle is significantly different for all three surfaces. Representative spectra of **(B)** XPS of the pristine DLC surface and **(C)** XPS of the pOEGMA terminated surface (N = 3).

and ablation was carried out with a sample translation rate of 0.5 mm/s. The sample was translated such as to ablate a series of parallel lines spaced 300 μm (**Figure 3**) or 250 μm (**Figure 5**) apart.

FIGURE 3 | (A) Raman spectrum of pristine DLC, (B) optical microscope images of the laser ablation track at 5 and 10 mW respectively (scale bar-is 40 μm) (C) Raman spectra of spots along the perpendicular of the laser ablation track at different distances of the ablation track (intensity of centre spectrum is scaled 10× compared to the other spectra) and (E) and (F) confocal image of green fluorescent-labelled laminin exposed laser ablated samples at 5 mW clearly revealing the laser ablation tracks, at ×10 and ×63 magnification (scale bars are 100 and 20 μm, respectively). Three independently produced samples were tested in these experiments.

Materials Characterisation
Contact Angle Measurements
The hydrophobicity of the surfaces was assessed by measuring the water contact angle. The angle formed by the baseline and the tangent to the drop profile at the three-phase point was measured using a Rame-Hart contact angle goniometer at room temperature. Ultrapure (18 MΩ) deionised water was used and two measurements were carried out on each of three replicate samples for each condition. Values were plotted as the mean plus or minus the standard deviation.
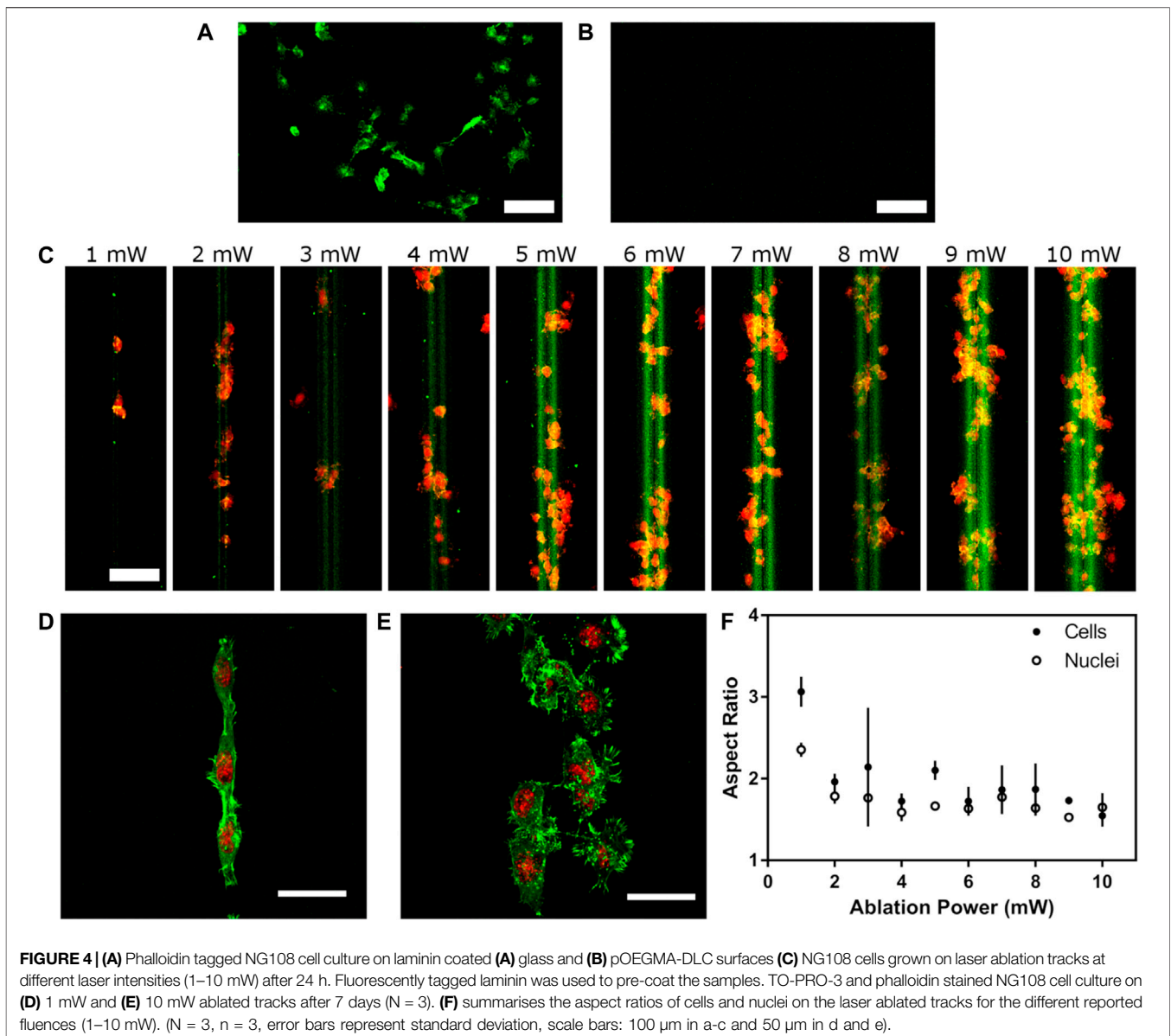
X-Ray Photoelectron Spectroscopy
Samples were analysed using a Kratos AXIS Ultra DLD instrument. Spectra were recorded using a monochromatised Al Kα X-ray source (1,486.6 eV) operating at a power of 150 W, whilst charging of the sample during irradiation was reduced by an internal flood gun. Each sample was analysed at an emission angle normal to the sample surface. Data processing, analysis and charge correction were carried out using CasaXPS software (Casa Software Ltd.). Component peaks within the recorded C (1s) spectra were deconvoluted and fitted to a mixed peak shape of 70% Gaussian/30% Lorentzian composition. The aliphatic hydrocarbon component of the C (1s) was set to 285.0 eV as an internal reference.

Raman Spectroscopy
Raman spectroscopy was performed on a Thermofisher DXR Raman Microscope. Spectra were obtained with a ×50 magnification microscope objective. The scan speed was 40 Hz (25 ms/spectrum) and spectra were a convolution of 100 scans with 5.4 mW at 532 nm.

FIGURE 4 | (A) Phalloidin tagged NG108 cell culture on laminin coated **(A)** glass and **(B)** pOEGMA-DLC surfaces **(C)** NG108 cells grown on laser ablation tracks at different laser intensities (1–10 mW) after 24 h. Fluorescently tagged laminin was used to pre-coat the samples. TO-PRO-3 and phalloidin stained NG108 cell culture on **(D)** 1 mW and **(E)** 10 mW ablated tracks after 7 days (N = 3). **(F)** summarises the aspect ratios of cells and nuclei on the laser ablated tracks for the different reported fluences (1–10 mW). (N = 3, n = 3, error bars represent standard deviation, scale bars: 100 μm in a-c and 50 μm in d and e).

Laminin Adsorption

Prior to seeding cells, the various samples were coated with polyornithine and laminin in order to promote neuronal cell adhesion. The samples were firstly sterilised by submersion in absolute methanol for 5 min before being allowed to dry in a biological safety cabinet. The samples were then incubated in poly-L-ornithine solution (200 μl, 0.002% w/w in PBS) for 1 h at 37°C, rinsed once in sterile deionised water and then incubated in a solution of laminin (0.05 mg/ml in PBS) for a further 1 h. The samples were finally rinsed once in PBS and used immediately for cell culture.

Cell Culture Studies
NG108 Cell Line

NG108-15 cells were maintained and expanded in a growth medium composed of Dulbecco's modified Eagle's medium supplemented with FBS (10% v/v), L-glutamine (2 mM), penicillin (100 U/ml), streptomycin (100 μg/ml) and amphotericin B (0.25 μg/ml). Cells were seeded onto either glass coated with poly-L-ornithine and laminin (positive control) or experimental samples at an initial density of 1×10^4 cells per cm^2 in complete growth medium. To induce terminal differentiation, the growth medium was replaced with a medium lacking FBS. Cells were cultured for either 24 h or 7 days at 37°C and 5% CO_2 after which they were fixed for microscopy.

Rat Embryonic Neural Stem Cells

Neural stem cell (NSC) growth medium consisted of Neurobasal (97 ml) supplemented with B27 (2 ml, variation without vitamin A), GlutaMax supplement (1 ml), penicillin/streptomycin (1 ml),
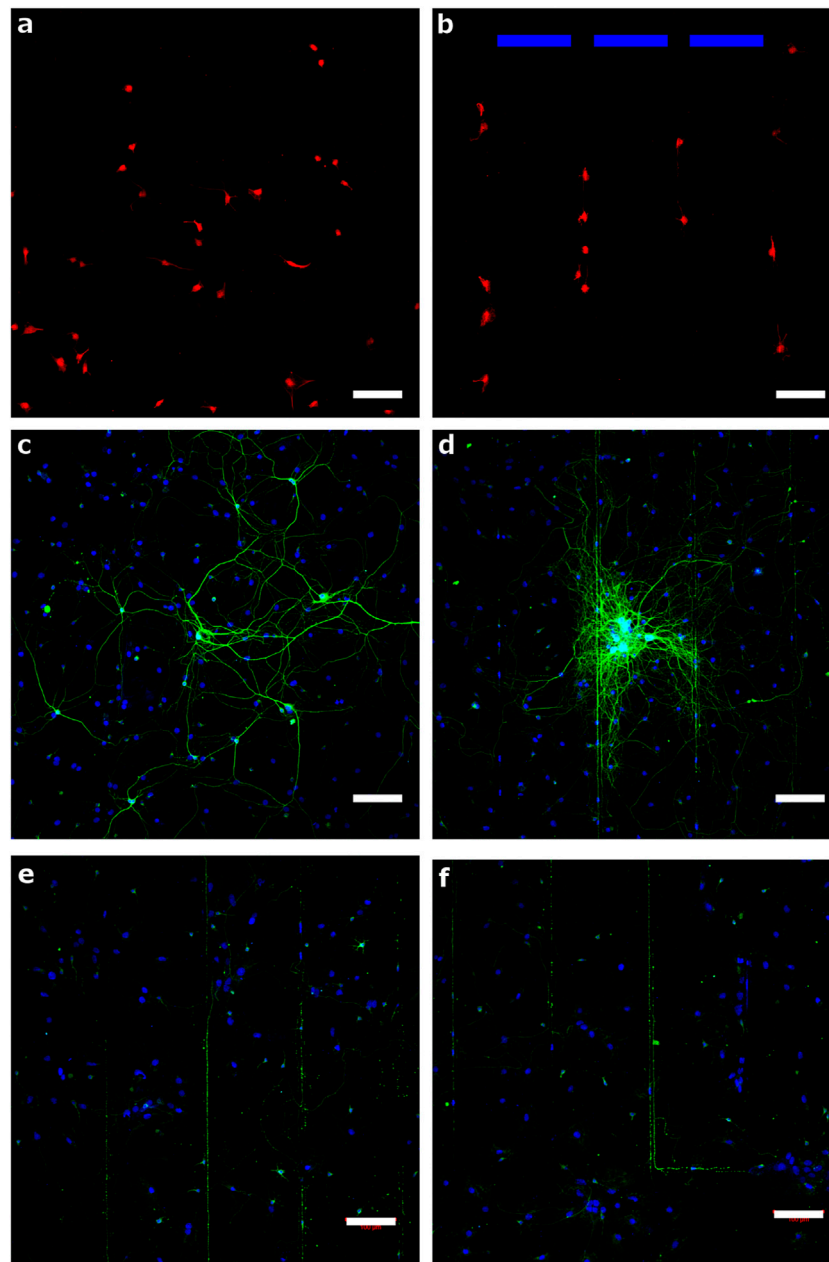
FIGURE 5 | Neural stem cell culture onto laminin/polyornithine coated glass at 2 days **(A)** and 25 days **(C)** and onto DLC with ablated tracks at a laser power of 1 mW at 2 days (b, blue bars indicate the regions between the ablation tracks) and 25 days **(D–F)**. Samples **(A)** and **(B)** are stained for nestin and samples **(C)** and **(D–F)** are stained for βIII-tubulin while the cell nuclei are stained with DAPI (scale bar = 100 μm).

epidermal growth factor (EGF, 20 μl, 0.1 mg/ml in PBS) and bFGF (20 μl, 0.1 mg/ml in PBS). NSC differentiation medium consisted of Neurobasal (97 ml) supplemented with B27 (2 ml, standard formulation including vitamin A) and GlutaMax supplement (1 ml). Non adherent culture plates were prepared as follows. Polyhydroxyethyl methacrylate (2 g, polyHEMA, bioreagent grade) was dissolved in a mixture of absolute ethanol (95 ml) and deionised water (5 ml) at 60°C for 1 h. After cooling, 0.5 ml of the polyHEMA solution was added

into each well of a standard tissue culture treated 6-well plate (Corning brand) and allowed to fully coat the culture surface. The excess solution was then removed and the plate was allowed to dry overnight.

NSCs were prepared using the neurosphere method from day 18 (E18) rat tissue. Fresh combined cortex and hippocampus (including subventricular zone) tissue from an E18 Sprague Dawley rat embryo was obtained pre-dissected from a commercial source (BrainBits Ltd., UK). The tissue was

subjected to enzymatic treatment in a solution of papain in hibernate E-Ca medium (8 mg in 4 ml) for 10 min at 30°C. The papain solution was then removed and replaced with hibernate E supplemented with B27 (4 ml). The tissue was then triturated rapidly for 30 s using a silanised glass Pasteur pipette. Undispersed tissue was allowed to settle for 1 min and the supernatant containing single cells was collected and centrifuged at $200 \times g$ for 1 min. The supernatant was discarded and the pellet gently redispersed in NSC growth medium (2 ml) using a 1 ml capacity micropipette. The viable cells were seeded in non-adherent tissue culture plates at a concentration of 30,000 cells per cm^2 in 4 ml of NSC growth medium per well (6-well plate). The cells were cultured at 37°C, 5% CO_2 and ambient oxygen. Multicellular neurospheres formed after approximately 2 days.

After 5–6 days in culture, by which time the neurospheres measured approximately 300–500 μm in diameter, the neurospheres were dissociated to form a suspension of single cells which were then seeded to the experimental samples. Dissociation was carried out enzymatically according to the following procedure. Neurospheres were transferred to a centrifuge tube and centrifuged at $100 \times g$ for 2 min. The supernatant was discarded and the neurospheres were gently redispersed in PBS (5 ml). The neurospheres were again centrifuged at $100 \times g$ for 2 min and the supernatant was discarded. Accutase (2 ml) was added and the neurospheres were gently redispersed. The neurospheres were incubated in the accutase for 10 min at room temperature before triturating 40 times with a 1 ml capacity micropipette against the bottom of the tube. NSC growth medium (8 ml) was added and the cell suspension was centrifuged at $100 \times g$ for 4 min and then at $200 \times g$ for a further 1 min. The supernatant was discarded and the cell pellet was redispersed in fresh NSC growth medium (1 ml) by gentle trituration with a 1 ml capacity micropipette to give a suspension of single cells.

Dissociated NSCs were seeded onto experimental samples (precoated as described in *Laminin Adsorption*) in NSC growth medium at a density of 10.000 cells per cm^2. After 2 days the cells were either fixed for staining and microscopy or else were allowed to spontaneously differentiate (favouring neurogenesis) by exchanging the medium for NSC differentiation medium (including B27 containing vitamin A and excluding EGF and bFGF). The differentiating cells were maintained in culture on the experimental samples for a further 21 days, refreshing half the differentiation medium every third day. The primary cells within the experiments reported in **Figure 5** were prepared from the same primary tissue.

Fluorescent Labelling and Immunocytochemistry

Immunocytochemistry was carried out using the following procedure. The culture medium was aspirated and the cells were gently rinsed once with PBS. The cells were then fixed for 10 min in 3% (w/v) formalin in PBS. A staining buffer was formulated containing 1% (v/v) adult goat serum, 0.1% (w/v) bovine serum albumin (BSA) and 0.1% (v/v) Triton X-100 in PBS. The samples were blocked against non-specific staining by pre-treating with staining buffer for 30 min. The buffer was then aspirated and replaced with the relevant primary antibody

dissolved in fresh blocking buffer at a dilution of 1/500. The samples were then incubated at 5°C overnight before rinsing three times with PBS. A suitable secondary antibody, conjugated to either AlexaFluor 488 or AlexaFluor 546, was then added to each sample dissolved in blocking buffer at a dilution of 1/500. The samples were incubated in the dark at room temperature for 1 h after which the antibody solution was removed. The samples were again rinsed three times with fresh PBS and the nuclei were stained with TO-PRO-3 or DAPI (300 nM) in PBS for 10 min. The samples were rinsed a final time in fresh PBS before being allowed to partially dry. The samples were then mounted in ProLong Gold antifade reagent which was allowed to cure overnight in the dark before microscopy was carried out.

Fluorescent labelling of f-actin to reveal cell morphology was carried out by staining with fluorescent derivatives of phalloidin. The procedure was the same as for immunocytochemistry except that the primary antibody was substituted for either FITC or TRITC-conjugated phalloidin diluted to 5 μg/ml in staining buffer and samples were incubated in the phalloidin solution for 1 h at room temperature. No secondary antibody was used.

Confocal microscopy was carried out using a Zeiss LSM 510 META upright confocal microscope and representative micrographs are presented.

Image Analysis

Image analysis of confocal micrographs was carried out using ImageJ software (NIH, United States) using calibrated dimensions. Cell and nucleus aspect ratios were measured using inbuilt semi-automated thresholding, segmentation and morphological measurement functions included in the standard distribution of the ImageJ package. Values were plotted as the mean plus or minus the standard deviation, based on average values from three images captured from each of three replicate samples giving a total of nine measurements ($n = 9$).

Statistical Analysis

Statistical analysis of contact angle values was carried out using GraphPad Prism software (GraphPad Software, San Diego, United States). Single-factor analysis of variance (ANOVA) was carried out in order to determine the probability (p) of apparent differences between conditions arising solely from experimental variance. *Post hoc* comparison of means (Tukey method) was carried out in order to reveal specific differences between pairs of conditions. The level of significance is highlighted as * for a p-value less than 0.05, ** for a p-value is less than 0.01 and *** for a p-value is less than 0.001.

RESULTS

Functionalisation by SI-ATRP

Upon functionalization of DLC with poly-oligoethylene glycol methacrylate (pOEGMA) brushes, a visibly coloured film was formed on the DLC surface. The surface properties and chemistry of the functionalised DLC were determined by measurement of

water contact angle and XPS spectra (**Figure 2**). The contact angle of the pristine DLC was 82° (±1.4) which dropped to 56° (±1.1) after functionalization by SI-ATRP (**Figure 2A**). The high resolution XPS spectrum (C 1s region) of pristine DLC (**Figure 2B**) showed the characteristic strong peak centred at 285 eV corresponding to the bulk state of the DLC. A small shoulder peak at higher binding energy was also identified after deconvolution, arising from carbon bound to oxygen indicating the presence of a thin oxide layer. Additionally, the carbon peak was deconvoluted into sp^2 (284.47 eV) and sp^3 (285 eV) carbon and arrived at 55.5% sp^3 and 44.5% sp^2 carbon, in line with the expectations for these DLC samples.

After functionalization with pOEGMA brushes by SI-ATRP, the XPS spectrum indicated three distinct chemical environments of carbon arising from the pOEGMA brush films (**Figure 2C**). The peak centred at 285 eV corresponds to the aliphatic polyacrylate backbone of the pOEGMA brush layer. The largest peak, centred at 286 eV corresponds to carbon bound to oxygen by a single bond and the peak at highest binding energy (289 eV) corresponds to the carboxyl/amide group. This is in line with expectations of the chemical structure of the pOEGMA brush layer (see **Figures 1B,C**). Additionally, the survey scan of the pOEGMA-functionalised DLC revealed only carbon and oxygen on the surface with a carbon to oxygen ratio of 2.23, close to the theoretical value of 2.15.

Laser Ablation

The Raman spectra reveal that the DLC chemical structure changes drastically upon ablation. This can be observed from a line scan from the ablation track to 50 μm away from the track at 5 and 10 mW laser power. The spectrum of the ablation track shows a clear sign of graphitisation of the DLC with two peaks at 1,360 and 1,590 cm^{-1} (respectively the D- and G-band). Upon deconvolution of the spectra it is also observed that the G-band peak position shifts from 1,565 to 1,590 cm^{-1} and the I_D/I_G ratio rises from 0.83 to 1.06 from the pristine DLC surface to the centre of the ablation track. The spectrum reverts to the pristine DLC spectrum at ~40 μm outside the ablation track for both laser powers. The microscope pictures of the ablation track also reveal a 3 μm wide ablation track surrounded by a wider region of less-reflective material. The width of this region varied linearly from 50 to 110 μm for a laser fluence of 1–10 mW. This could be identified either as a heat affected zone or a region of redeposited material (as will be further discussed in the discussions section). A substrate patterned at 5 mW was exposed to fluorescently labelled laminin, and example results are highlighted in **Figures 3E,F**. The laminin adsorption is solely confined to the region surrounding the laser ablation tracks and the adsorbed laminin signal has a width of 80 μm. Additionally, a 3.4 μm indentation can be observed on the cross-sectional image which shows the laser ablation track.

Culture of NG108-15 Neuronal Cell Line

NG108-15 cells were grown on glass coated with polyornithine and laminin as a positive control and pOEGMA-DLC as a negative control for cell adhesion. The cells were stained with fluorescent tagged phalloidin to stain filamentous actin and reveal their morphology. Fluorescence micrographs are shown in **Figure 4**. On coated glass the cells adopted a well spread, polygonal morphology with some small processes, as would be expected for this cell type (**Figure 4A**). In contrast, no cells were observed on the DLC-pOEGMA surfaces (**Figure 4B**), except in a small number of isolated regions where the pOEGMA brush coating had been accidentally damaged by handling (not shown). Fluorescence micrographs of NG108 cells growing on ablated DLC are shown in **Figure 4C**, with the cells labelled in red with TRITC-conjugated phalloidin and adsorbed laminin pre-labelled with FITC. On the ablated DLC the cells almost solely adhered on the regions surrounding the ablated tracks, while very few cells adhered on the areas away from the ablated tracks. Tracks were ablated using different laser powers, ranging from 1 to 10 mW. The width of the adsorbed region and the intensity of the green fluorescence corresponding to laminin adsorption appeared to vary with ablation laser power, with increasing degree of adsorption and width of adsorbed region with increasing power. The width of the region upon which the NG108 cells had adhered also appeared to increase with increasing ablation laser power. On the tracks ablated with the lowest power of 1 mW, only a small number of single cells were observed to have adhered. On the tracks ablated with the highest power of 10 mW, however, colonies of cells several cells wide were observed to have adhered on the tracks.

High resolution confocal micrographs of NG108 cells growing on DLC with tracks ablated using a low power of 1 mW and a high power of 10 mW are shown in **Figures 4D,E** respectively. On the track ablated at the high power of 10 mW, the cells not only adhered on a wider region but also adopted a more spread, polygonal morphology than on the narrower track ablated using the lower power of 1 mW. On the narrower track, the cells adopted a narrower, elongated morphology in line with the long axis of the track. Morphological image analysis of the cells was carried out on confocal images of the cells and also on the cell nuclei as stained with the far-red fluorescent nuclear stain TO-PRO-3. The results of the image analysis are shown in **Figure 4F**. A clear decrease in the aspect ratio of both cells and nuclei was observed with increasing laser ablation power resulting increasing width of adsorption/adhesion promoting regions surrounding the ablated tracks.

NG108 cells were allowed to undergo terminal differentiation for 7 days on the coated glass and the ablated DLC surfaces. After this time the cells were stained for βIII-tubulin (a cytoskeletal component and neuronal marker) *via* immunocytochemistry. Fluorescence micrographs are shown in **Figures 4G,H**. On coated glass many cells featured long processes (neurites) indicative of terminal differentiation of this cell type. On a DLC sample with tracks ablated with 1 mW laser power (**Figure 4H**), the cells had formed a densely confluent colony confined within the region surrounding the ablated track. The cells were too confluent to be able to identify any neurites but the cells apparently strongly expressed βIII-tubulin and were still confined within the ablated region even after 7 days.

Culture and Differentiation of Neural Stem Cells

NSCs were isolated from E18 rat brain tissue and expanded using the suspension neurosphere method in the presence of EGF and bFGF. After enzymatic dissociation, a suspension of single NSCs was seeded to laminin/polyornithine coated glass and DLC ablated at a laser power of 1 mW. After 2 days in NSC growth medium, some samples were fixed for microscopy and stained for nestin (a marker of the NSC phenotype) and the remaining samples were allowed to differentiate for a further 23 days in a growth medium supportive of neuronal differentiation. These samples were then fixed and stained for βIII-tubulin in order to reveal cells of a neuronal phenotype and to label nascent neurites. Fluorescence micrographs of nestin positive cells on coated glass and ablated DLC are shown in **Figure 5A** and **Figure 5B** respectively. On the coated glass surfaces, a uniform but sparse layer of cells had adhered. On the DLC ablated with 1 mW, however, the several cells that had adhered were constrained within the regions around the ablated tracks, in line with the spatial distribution observed with the NG108 cells. After 25 days, however, many more cells were observed growing on the coated glass (**Figure 5C**) and the ablated DLC (**Figure 5D**) than at the earlier time point, although a very significant proportion of the cells appeared to be negative for βIII-tubulin expression and appeared simply as cell nuclei revealed with the counterstain. However, a minority of the cells did stain brightly for βIII-tubulin and featured very long processes, longer than those produced by the NG108 cells in this experiment, which was indicative of having begun to differentiate down the neuronal lineage. No nestin expression was observed at this time point (images not shown). Some neuronal cells grew as multicellular colonies which projected very long processes away from the colonies. By this time point on the ablated DLC surfaces the cells were no longer constrained to the regions surrounding the ablated tracks, although some extended processes appeared to follow the paths of the ablated tracks. Indeed, **Figure 5** e and f indicate neurite lengths over 500 μm after 25 days and in particular **Figure 5F** indicates that the neurites follow closely the laser ablated tracks, in this image a track with a 90° turn is followed by a neurite.

DISCUSSION

Diamond-Like Carbon is a typical bio-inert surface which exhibits excellent haemocompatibility (Grill, 2003) and wear resistance (Hauert, 2004) and been investigated previously as a coating for stents (Maguire et al., 2005), for articulating surfaces for hip replacements (Saikko et al., 2001) and for coatings of dental abutment screws (Penkov et al., 2016). The use of DLC as a cell growth substrate for electronic interfaces would be enhanced by production techniques that enable patterned cell growth and modulation of the electronic properties of the coating in a patterned way. We have previously highlighted the use of phosphorus-doping of DLC and functionalisation via UV-irradiation for patterned cell growth (Kelly et al., 2008; Regan et al., 2010). Both of these approaches, doping and UV-irradiation, produce a negatively charged and hydrophilic surface, allowing for proteins a adhere and cells to attach. In this study we took a different approach via producing an antifouling coating on Diamond-Like Carbon via Si-ATRP, and consecutively ablating tracks on the surface to allow for patterned cell growth to occur.

The DLC surface was successfully functionalised with pOEGMA via ATRP as evidenced by XPS analysis. The XPS spectrum of the pOEGMA functionalised DLC resembles closely spectra of other pOEGMA functionalised surfaces reported in literature, for example on gold immobilised self-assembled monolayers (Alang Ahmad et al., 2010; Lilge and Schönherr, 2016) and silicon oxide (Ma et al., 2006; Hucknall et al., 2009). The carbon signal can be fitted with three components, corresponding to C-C/C-H (285 eV), C-O (286.5 eV) and O-C=O (289.0 eV) with a ratio of 0.70:0.22:0.08, which is close to the theoretical ratio of 0.73:0.20:0.09 for a 300 g/mol pOEGMA coating. This is confirmed by the survey scan results which detect only carbon and oxygen in the scan at a carbon to oxygen ratio of 2.23 (close to the theoretical value of 2.15 for pOEGMA). This is in line with previous reports for pOEGMA and indicate that no significant amount of Cu or Br ions is adsorbed in the pOEGMA brush layer (Shi et al., 2012). The XPS also indicates that the pOEGMA forms a conformal coating on the DLC surface thicker than 10 nm. Indeed, in Lilge and Schönherr (2016). coatings of 30 nm thickness were achieved for 1 h SI-ATRP reaction under similar conditions. The relative hydrophobicity/hydrophilicity of the surfaces was also assessed by contact angle measurement both before and after functionalization with pOEGMA brushes. DLC was found to be a relatively hydrophobic material with a water contact angle (WCA) of 82°, in excellent correspondence with previous reports of the DLC WCA (Yang et al., 2006; Kalin and Polajnar, 2014). Upon functionalization with pOEGMA brushes, the WCA decreased to 56°, indicating an increase in hydrophilicity and surface energy, in excellent agreement with a previously reported value of 58° on SI-pOEGMA brushes grown from self-assembled monolayers on gold (Lilge and Schönherr, 2016) and grown on poly (vinylidene fluoride) membranes. (Liu et al., 2007).

The DLC was ablated at a low power with a sub-nanosecond pulsed laser with a laser spot size of 3 μm. Given the write speed of 0.5 mm/s and a laser repetition rate of 45 kHz each spot size received 270 pulses. The laser fluence for 5 and 10 mW is 1.57 and 3.14 J/cm^2 respectively and given that the DLC is 4.75 μm thick the ablation rate is at least 18 nm/pulse for laser fluences above 1.57 J/cm^2 given that Raman lines arising from the underlying silicon substrate are observable (see discussion on Raman). This is in line with laser ablation rates on similar substrates with sub-nanosecond Nd-YAG lasers, for example an ablation rate is observed in between 20 and 40 nm/pulse for 150–300 ps 532 nm laser ablation of TiN at fluences of 1–3 J/cm^2 (Kononenko et al., 2000), and DLC ablation rates have been reported to be at least ~100 nm/pulse at that fluence (Kononenko et al., 2005).

Interestingly, the ablation track reveals a small physical ablation track of ~3 μm with a larger zone of ~50–80 μm affected the laser ablation. Two effects could cause the affected zone the creation of (i) a heat affected zone and (ii) redeposition of carbon on the initial surface. A heat affected zone as measured for similar laser settings does not extend for more than 10 μm from the ablation spot (Kononenko et al., 2005) the observed area is likely formed by redeposition which can affect a much larger area (~100 μm)

(Wang et al., 2007). This redeposition region is dependent on the laser power and changes linearly from 50 μm for 1 mW to 110 μm for 10 mW. The chemical structure of the DLC within the ablation track and the redeposition area was also studied with Raman spectroscopy. Both the Raman spectra within the ablation track at 5 and 10 mW laser power does indicate Raman absorption at 950 cm^{-1}. This indicates that ablation at these laser powers does remove the DLC layer to expose the underlying silicon substrate. The Raman spectrum of the DLC in the track at 5 mW on the other hand reveals graphitisation. The upwards shift of the G-band shifts from 1,565 to 1,590 cm^{-1} and the narrowing of its full width at half maximum from 152 to 112 cm^{-1} indicate a decrease of sp^3 fraction and this is also indicated by the increase in I(D)/I(G) ratio (Ferrari and Robertson, 2000; Dumitru et al., 2003; Kononenko et al., 2005). The redeposition of material on the substrate renders the antifouling coating ineffective in the area around the ablation track, as shown in **Figure 4**, and outside of the redeposition region there is no observable fouling.

The proposed surface patterning protocol lends itself to patterned growth of NG108s. NG108s grow solely on tracks and not on regions in between. As previously highlighted by XPS, the pOEGMA surfaces did not absorb any detectable amount of Copper or Bromine ions, so the patterned cell growth arose from a higher cell adhesion to the laser ablation tracks than the pOEGMA surface and any inherent toxicity because of remnant ions is unlikely. Shi et al. (2012) also studied pOEGMA surfaces for cell adhesion and highlighted the absence of Cu and Br on the treated surfaces. They also reported that the pOEGMA coating rendered planar substrates antifouling, while HeLa derived cells grew appreciably on nanostructured pOEGMA surfaces, indicating that there was no inherent cytotoxicity arising from the pOEGMA coatings (Shi et al., 2012). Tracks made with different laser powers present different width tracks for cell growth. This affects the aspect ratio of the cells, the cells grown on wider tracks have an aspect ratio of ~1.5 while cells grown on thinner tracks have a much higher aspect ratio, with the long axis of cells aligned along the track. Once cells become confluent they show clumped growth. Primary neurons show an initial attachment to the tracks. After 2 days the cells show excellent alignment with the pattern, after 25 days the neurites show excellent alignment with the tracks, while cells do grow also in between tracks, which indicates that the surface has not retained its non-fouling character after 25 days. These results are similar to the results observed by Kang et al. (2010). This study reports the growth of hippocampal neurons from E-18 Sprague/Dawley rat embryos on poly-L-lysine (PLL) patterned pOEGMA films and the cells grew along the PLL pattern for up to 10 days in vitro. The longer term cell culture results indicate a reduction of the antifouling properties of the DLC:pOEGMA surfaces produced in this study. This is in line with observations in other studies. Important to note is that this study uses polyethylene glycol methacrylate monomethyl ether for the brush surface, which produces superior antifouling properties compare to brushes produced by hydroxyl terminated PEGMA. The commercially available PEGMA (from Sigma) contains a significant amount of dimethacrylates, which results in crosslinks within the brushes, significantly reducing the antifouling properties (Ali and Stöver, 2004). Similar pOEGMA-based surfaces have been studied by Gautrot et al. (2010) who reported on the performance of 30 nm thick pOEGMA brushes, they observed negligible protein adhesion when these surfaces were exposed to FBS. Even when the pOEGMA surfaces were stored in ambient for 1 month the surfaces still showed low absorption. Our experiments indicate that the pOEGMA surfaces are stable for at least 7 days in cell culture media containing FBS, but show reduced antifouling properties when cells are cultured for a more extended period of time. Interestingly, the neurite outgrowth on the laser ablated samples follows the ablation tracks and long linear neurites can be observed on the samples. Even if the track is written with a 90° turn the neurite preferentially aligns with the track. This indicates that this method could be used for neurite patterning and alignment, which could be incorporated in an electrically active biointerface surface.

CONCLUSION

This study has shown that patterned neuronal cell growth and neurite extension can be achieved on DLC:pOEGMA patterned surfaces via laser ablation. The patterned cell growth can be sustained for a period of at least 7 days in vitro. The antifouling properties of the pOEGMA layer reduces over a period of 25 days in vitro, and the samples show cell significant adhesion on the non-ablated DLC:pOEGMA surface. After 25 days in vitro, long extended neurites can be observed to grow along the laser ablation tracks. The DLC layer within the laser ablated tracks graphitises as observed with Raman spectroscopy and will likely also provide conducting tracks within the electrically insulating DLC to interrogate the neuronal cells electrically.

DATA AVAILABILITY STATEMENT

The raw data supporting the conclusions of this article will be made available by the authors, without undue reservation.

AUTHOR CONTRIBUTIONS

JD, FC, A-AG and CC: conceptualization and project administration JD: data curation, formal analysis, and validation FC and CC: funding acquisition, resources, and supervision FC, A-AG and CC: investigation and methodology JD and FC: visualization and writing—original draft. A-AG, CC and FC: writing—review and editing. All authors contributed to the article and approved the submitted version.

FUNDING

REFERENCES

Alang Ahmad, S., Hucknall, A., Chilkoti, A., and Leggett, G. J. (2010). Protein Patterning by UV-Induced Photodegradation of Poly(oligo(ethylene Glycol) Methacrylate) Brushes. *Langmuir* 26 (12), 9937–9942. doi:10.1021/la100438d

Ali, M. M., and Stöver, H. D. H. (2004). Well-Defined Amphiphilic Thermosensitive Copolymers Based on Poly(ethylene Glycol) Monomethacrylate) and Methyl Methacrylate Prepared by Atom Transfer Radical Polymerization. *Macromolecules* 37 (14), 5219–5227. doi:10.1021/ma030485m

Ashfold, M. N. R., Claeyssens, F., Fuge, G. M., and Henley, S. J. (2004). Pulsed Laser Ablation and Deposition of Thin Films. *Chem. Soc. Rev.* 33 (1), 23–31. doi:10.1039/b207644f

Beck, R. J., Bitharas, I., Hand, D. P., Maisey, T., Moore, A. J., Shires, M., et al. (2020). Dynamics of Picosecond Laser Ablation for Surgical Treatment of Colorectal Cancer. *Sci. Rep.* 10 (1), 20261. doi:10.1038/s41598-020-73349-w

Bootkul, D., Supsermpol, B., Saenphinit, N., Aramwit, C., and Intarasiri, S. (2014). Nitrogen Doping for Adhesion Improvement of DLC Film Deposited on Si Substrate by Filtered Cathodic Vacuum Arc (FCVA) Technique. *Appl. Surf. Sci.* 310, 284–292. doi:10.1016/j.apsusc.2014.03.059

Chen, S., Li, L., Zhao, C., and Zheng, J. (2010). Surface Hydration: Principles and Applications toward Low-Fouling/nonfouling Biomaterials. *Polymer* 51 (23), 5283–5293. doi:10.1016/j.polymer.2010.08.022

Doyle, A. D., Wang, F. W., Matsumoto, K., and Yamada, K. M. (2009). One-Dimensional Topography Underlies Three-Dimensional Fibrillar Cell Migration. *J. Cel Biol.* 184 (4), 481–490. doi:10.1083/jcb.200810041

Dumitru, G., Romano, V., Weber, H. P., Pimenov, S., Kononenko, T., Hermann, J., et al. (2003). Laser Treatment of Tribological DLC Films. *Diamond Relat. Mater.* 12 (3), 1034–1040. doi:10.1016/s0925-9635(02)00372-2

Ferrari, A. C., and Robertson, J. (2000). Interpretation of Raman Spectra of Disordered and Amorphous Carbon. *Phys. Rev. B.* 61 (20), 14095–14107. doi:10.1103/physrevb.61.14095

Gautrot, J. E., Trappmann, B., Oceguera-Yanez, F., Connelly, J., He, X., Watt, F. M., et al. (2010). Exploiting the superior Protein Resistance of Polymer Brushes to Control Single Cell Adhesion and Polarisation at the Micron Scale. *Biomaterials* 31 (18), 5030–5041. doi:10.1016/j.biomaterials.2010.02.066

Green Marques, D., Alhais Lopes, P., T. de Almeida, A., Majidi, C., and Tavakoli, M. (2019). Reliable Interfaces for EGaIn Multi-Layer Stretchable Circuits and Microelectronics. *Lab. Chip* 19 (5), 897–906. doi:10.1039/c8lc01093e

Grill, A. (2003). Diamond-like Carbon Coatings as Biocompatible Materials-An Overview. *Diamond Relat. Mater.* 12 (2), 166–170. doi:10.1016/s0925-9635(03)00018-9

Hauert, R. (2004). An Overview on the Tribological Behavior of diamond-like Carbon in Technical and Medical Applications. *Tribology Int.* 37 (11), 991–1003. doi:10.1016/j.triboint.2004.07.017

Hochberg, L. R., Serruya, M. D., Friehs, G. M., Mukand, J. A., Saleh, M., Caplan, A. H., et al. (2006). Neuronal Ensemble Control of Prosthetic Devices by a Human with Tetraplegia. *Nature* 442 (7099), 164–171. doi:10.1038/nature04970

Hucknall, A., Rangarajan, S., and Chilkoti, A. (2009). In Pursuit of Zero: Polymer Brushes that Resist the Adsorption of Proteins. *Adv. Mater.* 21 (23), 2441–2446. doi:10.1002/adma.200900383

Ibrahim, S., Higgins, D. A., and Ito, T. (2007). Direct-Write Multiphoton Photolithography: A Systematic Study of the Etching Behaviors in Various Commercial Polymers. *Langmuir* 23 (24), 12406–12412. doi:10.1021/la7020066

Jakubowski, W., and Matyjaszewski, K. (2006). Activators Regenerated by Electron Transfer for Atom-Transfer Radical Polymerization of (Meth)acrylates and Related Block Copolymers. *Angew. Chem. Int. Ed.* 45 (27), 4482–4486. doi:10.1002/anie.200600272

Jeon, H., Schmidt, R., Barton, J. E., Hwang, D. J., Gamble, L. J., Castner, D. G., et al. (2011). Chemical Patterning of Ultrathin Polymer Films by Direct-Write Multiphoton Lithography. *J. Am. Chem. Soc.* 133 (16), 6138–6141. doi:10.1021/ja200313q

Kalin, M., and Polajnar, M. (2014). The Wetting of Steel, DLC Coatings, Ceramics and Polymers with Oils and Water: The Importance and Correlations of Surface Energy, Surface Tension, Contact Angle and Spreading. *Appl. Surf. Sci.* 293, 97–108. doi:10.1016/j.apsusc.2013.12.109

Kang, K., Kang, G., Lee, B. S., Choi, I. S., and Nam, Y. (2010). Generation of Patterned Neuronal Networks on Cell-Repellant Poly(oligo(ethylene Glycol) Methacrylate) Films. *Chem. Asian J.* 5 (8), 1804–1809. doi:10.1002/asia.200900761

Kelly, S., Regan, E. M., Uney, J. B., Dick, A. D., McGeehan, J. P., Mayer, E. J., et al. (2008). Patterned Growth of Neuronal Cells on Modified Diamond-Like Carbon Substrates. *Biomaterials* 29 (17), 2573–2580. doi:10.1016/j.biomaterials.2008.03.001

Kim, J. H., Shin, J. H., Shin, D. H., Moon, M.-W., Park, K., Kim, T.-H., et al. (2011). Comparison of diamond-like Carbon-Coated Nitinol Stents with or without Polyethylene Glycol Grafting and Uncoated Nitinol Stents in a Canine Iliac Artery Model. *Br. J. Radiol.* 84 (999), 210–215. doi:10.1259/bjr/21667521

Kononenko, T. V., Garnov, S. V., Pimenov, S. M., Konov, V. I., Romano, V., Borsos, B., et al. (2000). Laser Ablation and Micropatterning of Thin TiN Coatings. *Appl. Phys. A* 71 (6), 627–631. doi:10.1007/s003390000572

Kononenko, T. V., Kononenko, V. V., Pimenov, S. M., Zavedeev, E. V., Konov, V. I., Romano, V., et al. (2005). Effects of Pulse Duration in Laser Processing of Diamond-Like Carbon Films. *Diamond Relat. Mater.* 14 (8), 1368–1376. doi:10.1016/j.diamond.2005.02.009

Laube, N., Kleinen, L., Bradenahl, J., and Meissner, A. (2007). Diamond-Like Carbon Coatings on Ureteral Stents-A New Strategy for Decreasing the Formation of Crystalline Bacterial Biofilms? *J. Urol.* 177 (5), 1923–1927. doi:10.1016/j.juro.2007.01.016

Lilge, I., and Schönherr, H. (2016). Synthesis and Characterization of Well-Defined Ligand-Terminated Block Copolymer Brushes for Multifunctional Biointerfaces. *Polymer* 98, 409–420. doi:10.1016/j.polymer.2016.03.031

Liu, F., Du, C.-H., Zhu, B.-K., and Xu, Y.-Y. (2007). Surface Immobilization of Polymer Brushes onto Porous Poly(vinylidene Fluoride) Membrane by Electron Beam to Improve the Hydrophilicity and Fouling Resistance. *Polymer* 48 (10), 2910–2918. doi:10.1016/j.polymer.2007.03.033

Ma, H., Li, D., Sheng, X., Zhao, B., and Chilkoti, A. (2006). Protein-resistant Polymer Coatings on Silicon Oxide by Surface-Initiated Atom Transfer Radical Polymerization. *Langmuir* 22 (8), 3751–3756. doi:10.1021/la052796r

Maguire, P. D., McLaughlin, J. A., Okpalugo, T. I. T., Lemoine, P., Papakonstantinou, P., McAdams, E. T., et al. (2005). Mechanical Stability, Corrosion Performance and Bioresponse of Amorphous Diamond-Like Carbon for Medical Stents and Guidewires. *Diamond Relat. Mater.* 14 (8), 1277–1288. doi:10.1016/j.diamond.2004.12.023

Matyjaszewski, K., Jakubowski, W., Min, K., Tang, W., Huang, J., Braunecker, W. A., et al. (2006). Diminishing Catalyst Concentration in Atom Transfer Radical Polymerization with Reducing Agents. *Proc. Natl. Acad. Sci.* 103 (42), 15309–15314. doi:10.1073/pnas.0602675103

Matyjaszewski, K., Dong, H., Jakubowski, W., Pietrasik, J., and Kusumo, A. (2007). Grafting from Surfaces for "Everyone": ARGET ATRP in the Presence of Air. *Langmuir* 23 (8), 4528–4531. doi:10.1021/la063402e

Menegazzo, N., Kahn, M., Berghauser, R., Waldhauser, W., and Mizaikoff, B. (2011). Nitrogen-Doped Diamond-Like Carbon as Optically Transparent Electrode for Infrared Attenuated Total Reflection Spectroelectrochemistry. *Analyst* 136 (9), 1831–1839. doi:10.1039/c0an00503g

Ohtake, N., Hiratsuka, M., Kanda, K., Akasaka, H., Tsujioka, M., Hirakuri, K., et al. (2021). Properties and Classification of Diamond-Like Carbon Films. *Materials (Basel)* 14 (2), 315. doi:10.3390/ma14020315

Penkov, O. V., Pukha, V. E., Starikova, S. L., Khadem, M., Starikov, V. V., Maleev, M. V., et al. (2016). Highly Wear-Resistant and Biocompatible Carbon Nanocomposite Coatings for Dental Implants. *Biomaterials* 102, 130–136. doi:10.1016/j.biomaterials.2016.06.029

Polikov, V. S., Tresco, P. A., and Reichert, W. M. (2005). Response of Brain Tissue to Chronically Implanted Neural Electrodes. *J. Neurosci. Methods* 148 (1), 1–18. doi:10.1016/j.jneumeth.2005.08.015

Pu, J.-C., Wang, S.-F., Lin, C.-L., and Sung, J. C. (2010). Characterization of Boron-Doped Diamond-Like Carbon Prepared by Radio Frequency Sputtering. *Thin Solid Films* 519 (1), 521–526. doi:10.1016/j.tsf.2010.07.018

Regan, E. M., Uney, J. B., Dick, A. D., Zhang, Y., Nunez-Yanez, J., McGeehan, J. P., et al. (2010). Differential Patterning of Neuronal, Glial and Neural Progenitor Cells on Phosphorus-Doped and UV Irradiated Diamond-Like Carbon. *Biomaterials* 31 (2), 207–215. doi:10.1016/j.biomaterials.2009.09.042

Rodriguez-Emmenegger, C., Hasan, E., Pop-Georgievski, O., Houska, M., Brynda, E., and Alles, A. B. (2012). Controlled/Living Surface-Initiated ATRP of

Antifouling Polymer Brushes from Gold in PBS and Blood Sera as a Model Study for Polymer Modifications in Complex Biological Media. *Macromol. Biosci.* 12 (4), 525–532. doi:10.1002/mabi.201100425

Saikko, V., Ahlroos, T., Calonius, O., and Keränen, J. (2001). Wear Simulation of Total Hip Prostheses with Polyethylene against CoCr, Alumina and diamond-like Carbon. *Biomaterials* 22 (12), 1507–1514. doi:10.1016/s0142-9612(00)00306-9

Shi, X., Wang, Y., Li, D., Yuan, L., Zhou, F., Wang, Y., et al. (2012). Cell Adhesion on a POEGMA-Modified Topographical Surface. *Langmuir* 28 (49), 17011–17018. doi:10.1021/la303042d

Singh, A., Ehteshami, G., Massia, S., He, J., Storer, R. G., and Raupp, G. (2003). Glial Cell and Fibroblast Cytotoxicity Study on Plasma-Deposited Diamond-Like Carbon Coatings. *Biomaterials* 24 (28), 5083–5089. doi:10.1016/s0142-9612(03)00424-1

Srinivasan, S., Tang, Y., Li, Y. S., Yang, Q., and Hirose, A. (2012). Ion Beam Deposition of DLC and Nitrogen Doped DLC Thin Films for Enhanced Haemocompatibility on PTFE. *Appl. Surf. Sci.* 258 (20), 8094–8099. doi:10.1016/j.apsusc.2012.04.178

Surman, F., Riedel, T., Bruns, M., Kostina, N. Y., Sedláková, Z., and Rodriguez-Emmenegger, C. (2015). Polymer Brushes Interfacing Blood as a Route Toward High Performance Blood Contacting Devices. *Macromol. Biosci.* 15 (5), 636–646. doi:10.1002/mabi.201400470

Wang, J.-S., and Matyjaszewski, K. (1995). Controlled/"Living" Radical Polymerization. Atom Transfer Radical Polymerization in the Presence of Transition-Metal Complexes. *J. Am. Chem. Soc.* 117 (20), 5614–5615. doi:10.1021/ja00125a035

Wang, Y., Dai, N., Li, Y., Wang, X., and Lu, P. (2007). Ablation and Cutting of Silicon Wafer and Micro-mold Fabrication Using Femtosecond Laser Pulses. *J. Laser Appl.* 19 (4), 240–244. doi:10.2351/1.2795754

Yang, P., Huang, N., Leng, Y. X., Yao, Z. Q., Zhou, H. F., Maitz, M., et al. (2006). Wettability and Biocompatibility of Nitrogen-Doped Hydrogenated Amorphous Carbon Films: Effect of Nitrogen. *Nucl. Instr. Methods Phys. Res. Section B: Beam Interact. Mater. Atoms* 242 (1), 22–25. doi:10.1016/j.nimb.2005.08.081